Analysis of Cell-Target Encounter by Random Filopodial Projections

Helen M. Buettner
Dept. of Chemical and Biochemical Engineering, Rutgers University, Piscataway, NJ 08855

Dynamic projections from the surface of many motile cell types provide for variable contact with the extracellular environment and can be important in regulating cell migration events. For example, during nerve development and regeneration, the sensory motile tip of the axon exhibits long, slender filopodia projecting from the growth cone periphery. Extension and retraction of these filopodia continually remodel the points of contact between axon and surroundings. Experimental studies show that filopodial contact with specific extracellular features can guide subsequent growth cone migration, suggesting a potentially important means of engineering nerve growth to repair nerve injury or construct biological neural networks. A simulation model is presented of the dynamic filopodial structure on the nerve growth cone based on recent experimental characterization. The model is analyzed to obtain quantitative relationships between average filopodial characteristics, which are commonly measured experimental quantities, and the underlying parameters of individual filopodium dynamics. It is then applied to simulate encounter between a growth cone and its target due to filopodial dynamics alone. Filopodial contribution to growth cone-target encounter is summarized in terms of a mean encounter time that is reminiscent of a first passage time for a diffusing particle. The parametric relationships in this study provide a basis for further investigation of filopodial-mediated mechanisms in nerve growth and other cellular processes.

Introduction

Many biological cells exhibit transient protrusions of the cell surface called filopodia, which appear randomly in space and time and are thought to serve as sensors of the extracellular environment. Events such as the homing of a growing nerve axon to a precise location in the embryo (O'Connor et al., 1990) or the advance of the archenteron in sea urchin morphogenesis (Hardin and McClay, 1990) are triggered by filopodial contact with specific cues in the surroundings. The link between filopodial contact and the occurrence of these events offers a potentially valuable means of controlling cellular behavior through appropriate cue placement or regulation of filopodial activity. Elucidation of specific rules for exploiting this relationship would be greatly facilitated, however, by a quantitative model of filopodial dynamics that can be used to investigate the fundamental mechanisms underlying filopodial mediated processes. As an initial step in developing such a framework, this article addresses filopodial involvement in the process of nerve growth and regeneration.

Filopodia are concentrated at the growth cone, which is the expanded, sensory-motile tip of the nerve axon where axonal growth occurs and pathfinding decisions are made (Figure 1a). Typically about 0.1 μm wide and up to 50 μm or more in length, filopodia are essential to normal axonal growth. Growth cones deprived of filopodia by pharmacological treatment trace out distorted trajectories in tissue culture (Marsh and Letourneau, 1984) and are unable to follow appropriate developmental pathways in the embryo (Chien et al., 1993; Bentley and Toroian-Raymond, 1986). Considerable work suggests that filopodia sample their surroundings for discrete cues that guide the growth cone along the path of axonal extension in both *in vivo* (Oakley and Tosney, 1993; Myers and Bastiani, 1993a,b; O'Connor et al., 1990; Caudy and Bentley, 1986) and *in vitro* (Clark et al., 1993; Hammarback and Letourneau, 1986) environments. Filopodial contact with specific extracellular features can serve to attract or repel the growth cone in a stereotypical fashion, as illustrated for several examples in Figure 2.

Despite much experimental effort and a variety of systems

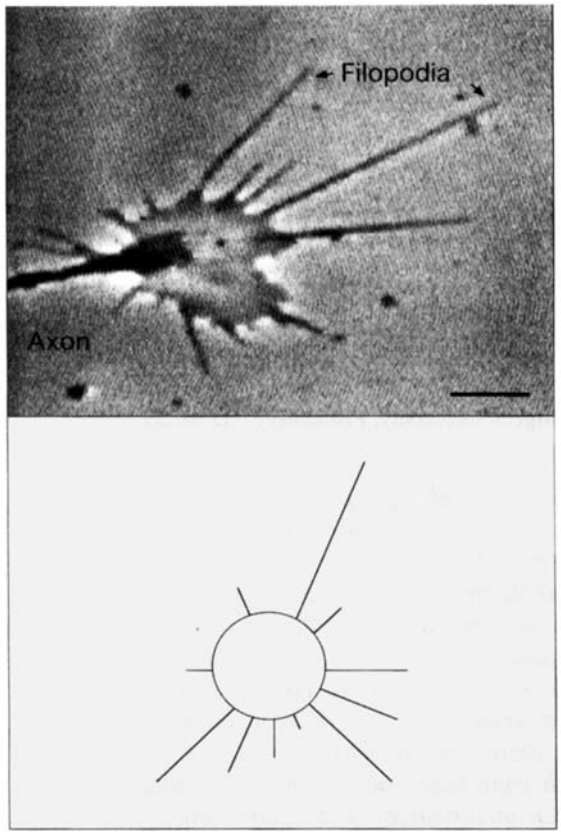

Figure 1. (a) Growth cone of a rat neuron in tissue culture; (b) simulated growth cone with the same mean characteristics as the experimental growth cone.

$\nu = 0.085$, $r_e = 0.049$ μm/s, $r_r = 0.028$ μm/s, $\langle N \rangle = 16$, $\langle L \rangle = 3.3$ μm, $\langle T_{max} \rangle = 70$ s; scale bar = 3 μm.

in which growth cone filopodial behavior can be observed, the quantitative link between filopodium-cue contact and growth cone response has been difficult to elucidate. The greatest challenge is posed by the complex nature of filopodial dynamics, particularly their randomness. Measurement of filopodial dynamics on growth cones of chick and rat neurons showed that filopodia initiate at random time intervals and positions around the growth cone, and extend to random lengths before retracting (Buettner et al., 1994). Thus the filopodial structure of the growth cone is continually modified, and the number and lengths of filopodia on a growth cone vary randomly with time. When filopodia are sparse, as is typically the case, filopodial sensing events that require direct contact with discrete targets become probabilistic in nature. The observation of quantitative trends in these events requires sample numbers that are not often feasible.

An alternative is to develop a simulation model that enables computer experiments on growth cone and filopodial behavior. Recently, a model of dynamic filopodial structure has been proposed based on experimental parameters of individual filopodium behavior (Buettner et al., 1994). The model is used here to investigate growth cone-target encounter for the limiting case in which the growth cone maintains a fixed distance from the target so that encounter occurs as a result of filopodial extension alone. A semi-infinite target is considered, with the target extending infinitely in all three directions away from the growth cone (Figure 3). This

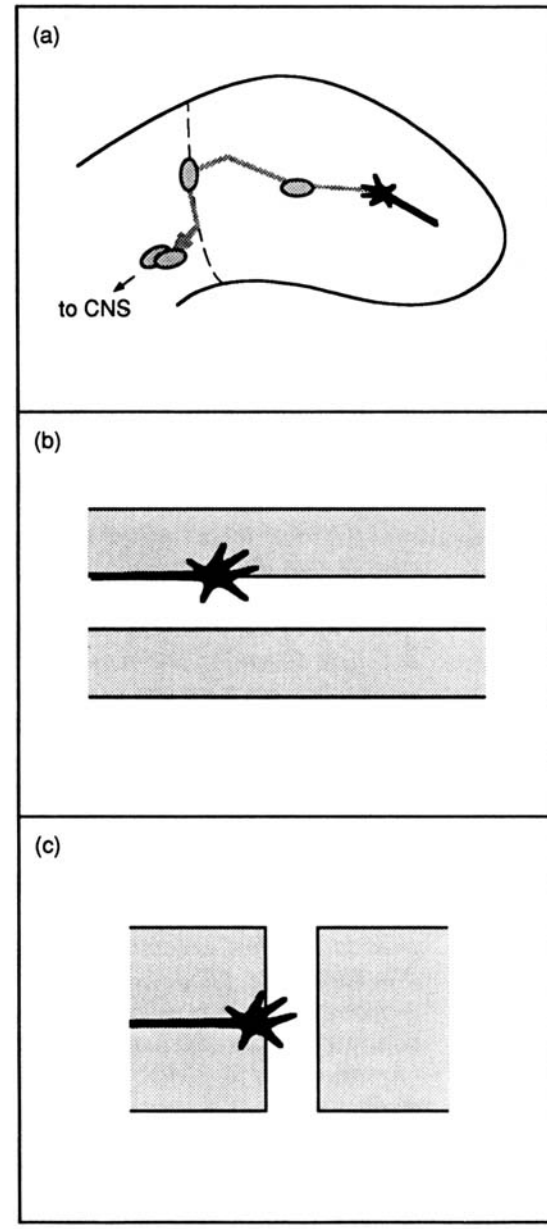

Figure 2. Paradigms of growth cone migration mediated by filopodial encounter.

(a) In the limb bud of the grasshopper embryo, pioneer axon growth inward towards the central nervous system (CNS) occurs along a path (grey line) marked by "guidepost" cells (stippled), a series of targets which filopodia must contact to properly orient growth cone migration (O'Connor et al., 1990; Bentley and Toroian-Raymond, 1986; Caudy and Bentley, 1986; Bentley and Caudy, 1983). The dashed line represents a segment boundary along which the growth cone migrates for a time as well; (b) growth cones advancing along a track of one substrate (stippled) migrate across a less favorable strip (plain) to a second track of the first substrate after filopodial contact with it (unpublished observations) and do not migrate across unfavorable strips that filopodia cannot bridge (Clark et al., 1993); (c) a growth cone advancing on a permissive substrate (stippled) will pause at a nonpermissive border until filopodial contact with a neighboring permissive region enables it to bridge the nonpermissive strip (Hammarback and Letourneau, 1986).

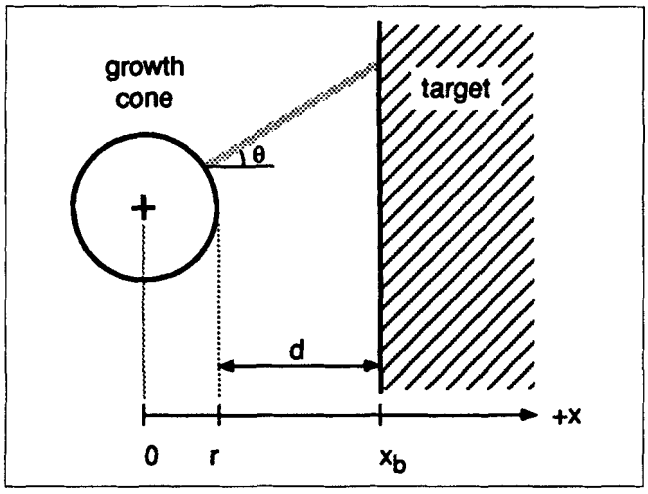

Figure 3. Growth cone-target geometry employed in the simulation.

The growth cone was approximated as a circle of radius r centered at the origin of a rectangular coordinate system. The target was separated from the leading front of the growth cone by a distance d, with its left boundary at $x = x_b$ ($= r + d$) and its other three boundaries at $x \to \infty$, $y \to \pm\infty$. Filopodia projected radially from the growth cone periphery at an angle θ, requiring $\theta < \pm \pi/2$ and an extension length of $d/\cos\theta$ to contact the target.

represents the situation, found both *in vivo* and *in vitro*, in which the growth cone approaches a target much larger than itself. Examples include extended regions of non-neuronal cells or other cues in the embryonic tissue (O'Connor et al., 1990; Dodd and Jessell, 1988), a fascicle of other neurites (Myers and Bastiani, 1993a), and chemical or physical regions of a micropatterned substrate (Clark et al., 1993, 1987; Hammarback and Letourneau, 1986; Lom et al., 1993). Encounter is characterized in terms of a mean encounter time, and its functional dependence on the parameters of filopodial dynamics and growth cone-target distance is determined. The results indicate that filopodial-target encounter in the absence of growth cone migration depends on both geometry and kinetics, a more complex dependence than has generally been assumed. Additionally, large variations in parametric sensitivity within the parameter space observed for filopodial dynamics in neuronal growth support the current hypothesis that filopodial contact may mediate a wide range of pathfinding behavior by the growth cone.

Methods

Simulation model of filopodial dynamics

Since the development of the simulation model used for this work has been described in detail elsewhere (Buettner et al., 1994), only the essential points of the model are reviewed here. In brief, the dynamic filopodial structure on a simulated growth cone was modeled using a Monte Carlo approach to generate individual filopodia at random intervals of time. The tip position of each filopodium generated was traced throughout its life cycle, which consisted of a single, continuous phase of extension to a random maximum length followed by retraction back to the initiation point. The quantitative characteristics of these events are based directly on the experimental measurements of Buettner et al. (1994) and are summarized as follows:

(1) Filopodial initiation is a Poisson event with a mean initiation rate of ν; the distribution of the number of filopodia generated per unit time interval Δt is given by

$$p(N) = (\nu\Delta t)^N (e^{-\nu\Delta t})/N!, \quad N = 0,1,2,\ldots \tag{1}$$

(2) The time T_{max} for a filopodium to reach maximum extension is described by the gamma distribution

$$p(T_{max}) = \beta^{\alpha}(T_{max})^{\alpha-1}\exp(-\beta T_{max})/\Gamma(\alpha), \tag{2}$$

where the parameters α and β determine the shape of the distribution and are related to the mean $\langle T_{max}\rangle$ through the expression

$$\langle T_{max}\rangle = \alpha/\beta. \tag{3}$$

Note that the choice of the gamma distribution is empirical and that other distributions with the same shape could be used. The simulation results are unaffected by this choice since they depend only on the shape of the distribution.

(3) Filopodium length L depends linearly on the rates of extension and retraction, yielding

$$L = r_e t \qquad t \le T_{max} \tag{4a}$$

$$L = L_{max} - r_r(t - T_{max}) \quad t \ge T_{max} \tag{4b}$$

where L_{max} is the length at $t = T_{max}$, i.e., the length at maximum extension.

(4) Filopodia extend radially from the growth cone periphery, assumed to be circular, with the x- and y-coordinates of the filopodium tip given by

$$x_t = x_o + L\cos\theta \quad \text{and} \quad y_t = y_o + L\sin\theta, \tag{5}$$

where (x_o, y_o) is the point of initiation and θ is the initiation angle relative to the leading front of the growth cone (see Figures 3 and 4).

(5) The point of initiation (x_o, y_o) of successive filopodia varies randomly around the growth cone periphery, but exhibits relatively uniform spacing between the filopodia present at any given time. This condition is achieved by dividing the growth cone into a number of sectors defined by the integer nearest to the average number of filopodia per growth cone. As a filopodium is initiated, it is assigned with uniformly random probability to an unoccupied sector. If all sectors are occupied, the filopodium is assigned, again with uniformly random probability, to one of the occupied sectors. However, all sectors must fill with n filopodia before the $(n+1)$st is added to any sector. In this placement scheme, all filopodia within a given sector are placed at its center and thus project at the same angle (Figure 4). A realization of the resulting simulated growth cone is shown in Figure 1b and can be compared to a real growth cone with the same statistical characteristics in Figure 1a.

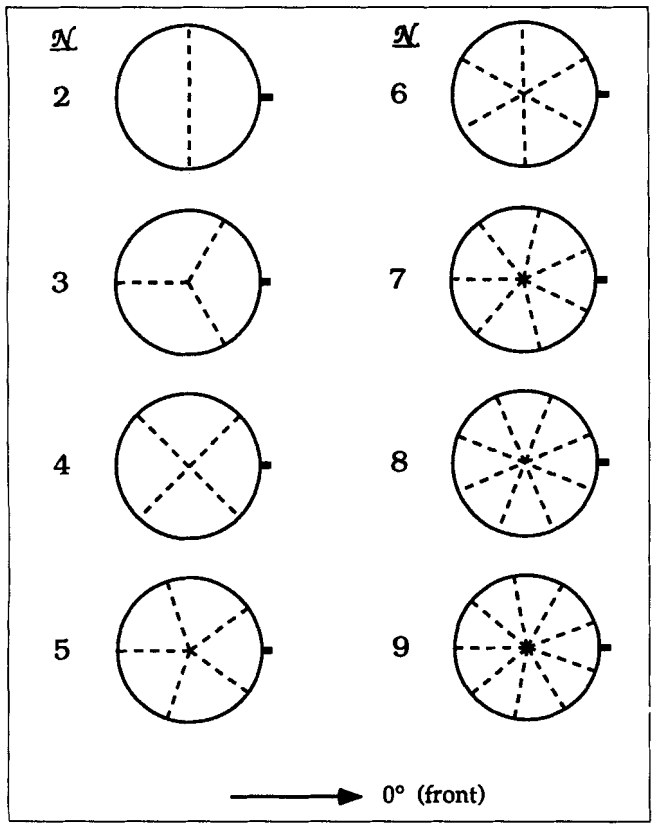

Figure 4. Filopodial orientation scheme.

The growth cone was divided into a number of sectors, $\mathfrak{N}$ equal to the mean number of filopodia per growth cone, rounded off to the nearest integer. Filopodia were placed at the center of a given sector, with one sector always centered at 0° so that a filopodium placed in that sector contacted the target by extending a minimum distance d. Filopodia were assigned to sectors at random as described in the text.

Simulation of filopodium-target encounter

Growth cone-target encounter was characterized in terms of a mean encounter time representing the mean time in a population of growth cones for at least one filopodium per growth cone to contact the target

$$\langle t \rangle = (1/N)\Sigma t_i, \tag{6}$$

where t_i is the time to initial contact by the ith growth cone and N is the number of growth cones in the population. The system geometry was defined by a circular growth cone of radius r at the origin of a rectangular coordinate system with the target located at $x \geq x_b$ and extending to $\pm\infty$ in the y-direction (Figure 3). The simulation was incremented at constant time steps of 1 s, two orders of magnitude less than the mean filopodial lifetime and at least one order of magnitude less than most encounter times. At each time step, the positions of all filopodial tips projecting at an angle $< \pi/2$ were calculated and compared to the target boundary. If $x_t > x_b$, the encounter time for that growth cone was recorded and the simulation looped to the next growth cone. The average encounter time for 1,000 growth cones with a given set of filopodial parameters (fixed ν, r_e, r_r, α, β) was obtained from each run. Runs were repeated using new random number seeds until the standard deviation was less than 5% of the mean encounter time for all runs at a given set of conditions. The first 10,000 s of filopodial activity for each growth cone was discarded to ensure that a steady-state filopodial configuration had been achieved before testing for encounter.

The parameter space for the simulation was set to encompass the range of values reported in the literature for ν, r_e, and r_r while maintaining the mean number and length of filopodia per growth cone $\langle N \rangle$ and $\langle L \rangle$ within their experimental ranges (Table 1). Since very little information is available on the shape parameters α and β or mean of the gamma distribution of maximum extension times, a single representative value of $\alpha/\beta = 100$ s (Buettner et al., 1994) was used throughout. Most encounter times are reported for $\alpha = 2$, with several included at $\alpha = 5$ for comparison.

Results

Average filopodial number and length

Rules 1 through 3 of the simulation model provide analytical relationships between the mean number and length of filopodia per growth cone and the dynamic parameters ν, r_e, r_r, α, β. The mean filopodial number per growth cone $\langle N \rangle$ is given by the average number of filopodia initiated during the mean filopodium lifetime $\langle T_L \rangle$

$$\langle N \rangle = \nu \langle T_L \rangle \tag{7}$$

where $\langle T_L \rangle = \langle T_{\max} \rangle + \langle T_r \rangle$, the sum of the mean time to reach maximum extension $\langle T_{\max} \rangle$, and the mean retraction time $\langle T_r \rangle$. From Eq. 4, $\langle T_{\max} \rangle = \langle L_{\max} \rangle / r_e$, where $\langle L_{\max} \rangle$ is the mean filopodium length at maximum extension. Since $\langle L_{\max} \rangle$ also represents the total retraction length, the mean retraction time is $\langle T_r \rangle = \langle L_{\max} \rangle / r_r$. Substituting these expressions into Eq. 7 yields

$$\langle N \rangle = \nu \langle L_{\max} \rangle (1/r_e + 1/r_r) \tag{8a}$$

Table 1. Experimental and Simulation Model Parameter Values

Parameter	Exp. Measured Range	Values Used in Simulation*	Experimental Data Sources**
ν (s^{-1})	0.01–0.06	0.01–0.05	2, 3
r_e (μm/s)	0.01–0.26	0.05–0.20	1–3, 9–12
r_r (μm/s)	0.01–0.27	0.05–0.20†	2, 3, 9, 12
α	0.80–5.0	2.0, 5.0	3
β (s^{-1})	0.01–0.05	0.02, 0.05‡	3
$T_{\max}$ (s)	70–155	100	3
$\langle N \rangle$	4–25	2–25	2–9
$\langle L \rangle$ (μm)	2–12	3–15	2, 5–8

*Values above the dashed line represent primary model parameters; model values below the line are determined from the preceding five parameters through Eqs. 3, 8, and 11, respectively.

**1. Argiro et al. (1985); 2. Bray and Chapman (1985); 3. Buettner et al. (1994); 4. Cohan (1989); 5. Hammarback and Letourneau (1986); 6. Letourneau (1979); 7. Letourneau et al. (1986); 8. Letourneau et al. (1987); 9. Myers and Bastiani (1993b); 10. O'Connor et al. (1990); 11. Sheetz et al. (1990); 12. Sheetz et al. (1992).

†Subject to the constraint that $1 \leq r_e/r_r \leq 4$, based on the experimental data cited.

‡Subject to the constraint that $\alpha/\beta = 100$ s.

or

$$\langle N \rangle = \nu(\alpha/\beta)(1 + r_e/r_r) \tag{8b}$$

In addition, the instantaneous number of filopodia per growth cone is described by a Poisson distribution (Morse, 1958)

$$p(N) = [\langle N \rangle^N \exp(-\langle N \rangle)/N!] \tag{9}$$

and thus has a variance equal to its mean

$$\sigma_N^2 = \langle N \rangle, \tag{10}$$

Equations 8 through 10 represent characteristics of a single growth cone observed over a long period of time or of a population of growth cones observed at a given instant in time.

The mean filopodial length per growth cone can be derived (see Appendix) to obtain the expression

$$\langle L \rangle = (1 - p_o) r_e(\alpha + 1)/2\beta, \tag{A17}$$

where $p_o = \exp(-\langle N \rangle)$ is the probability that no filopodia are present on the growth cone, obtained by setting $N = 0$ in Eq. 9. Multiplying the righthand side by α/α yields

$$\langle L \rangle = (1 - p_o)\langle L_{\max} \rangle(\alpha + 1)/2\alpha. \tag{11}$$

For values of $\langle N \rangle \geq 5$, $p_o \approx 0$, giving

$$\langle L \rangle = \langle L_{\max} \rangle(\alpha + 1)/2\alpha. \tag{12a}$$

or

$$\langle L \rangle = r_e(\alpha + 1)/2\beta. \tag{12b}$$

Effect of mean filopodial length $\langle L \rangle$ on encounter time

For each set of filopodial parameters, encounter times were obtained for distances d ranging from 1 to 6 times the mean filopodial length, given by Eq. 12, yielding distances ranging from 3.75 to 90 μm. When plotted against the dimensionless distance $d/\langle L \rangle$ all encounter times for a given initiation rate ν and ratio of extension to retraction r_e/r_r collapsed to a single curve. Thus, the encounter time is independent of the absolute values of r_e and r_r within the range examined. All encounter times are reported below as a function of the dimensionless distance.

Effect of initiation rate ν and ratio of extension to retraction rates r_e/r_r

Increasing either the rate of initiation ν or the ratio of extension to retraction rates r_e/r_r serves to increase the average number of filopodia per growth cone (see Eq. 8b). However, these two parameters have opposing effects on the mean encounter time. As illustrated in Figure 5, encounter time decreases with increasing ν and increases with increasing r_e/r_r. The reasons for both effects center on the rate at which the front half of the growth cone can generate a filopodium long enough to contact the target. Coupled to this are geometrical considerations imposed by the placement scheme used to position the filopodia around the growth cone. The simplest case occurs with changes in r_e/r_r at constant ν. Referring to Figure 6a, at $\nu = 0.01$ for example, as r_e/r_r increases from 1 to 4, $\langle N \rangle$ increases from 2 to 5. However, as illustrated in Figure 4, the number of sectors in which filopodia have access to the target remains at one for $\langle N \rangle$ equal to 2 through 4. The *fraction* of filopodia with access to the target decreases over that range from 0.5 at $\langle N \rangle = 2$ to 0.25 at $\langle N \rangle = 4$, since filopodia are distributed evenly among the sectors over a period of time. Even at $\langle N \rangle = 5$, where 3 filopodia face the target, those at $\pm 72°$ must travel much further to reach the target [a distance of $d/\cos(72°) = 3.24d$], so that encounter effectively relies on the filopodium at 0° which represents only 20% of the total number of filopodia generated on the growth cone. Thus, encounter time changes significantly over this range of conditions. Increasing the rate of initiation at constant r_e/r_r results in the same changes in filopodial configuration due to the increase in filopodial number, but the diminished fraction of filopodia at the front of the growth cone is offset by their greater rate of appearance. Considering the case of $r_e/r_r = 1$, at $\nu = 0.01$, 50% of the filopodia generated occupy the position at 0°. If ν is increased to 0.02, only 25% of the filopodia occupy that position, but they appear at twice the rate so that the same total number is placed at 0° over a given period of time, and the encounter time remains the same between these two cases. As the number of filopodia per growth cone increases up to about 8 or more and the filopodia are placed at smaller angular intervals, the frontward facing filopodia on either side of the 0° position begin to contribute non-negligibly to the probability of encounter, and the mean encounter time becomes more sensitive to changes in ν. However, at large $\langle N \rangle$ and constant ν, changes in filopodial number have a diminishing effect on the fraction of filopodia that contribute to target encounter.

A concise summary of the simulation results for $d/\langle L \rangle > 2$ was obtained by fitting the mean encounter times generated for each parameter set (ν, r_e/r_r, α, β) to an exponential curve of the form

$$\langle t \rangle = b \exp(a^{d/\langle L \rangle}) \tag{13}$$

Not all parameter sets yielded distinct curves. Simulation results from parameter sets yielding identical encounter times were thus combined into groups, as shown in Figure 6b, and Eq. 13 was fit to the combined data within each group. The fitted values of a, b and an estimate of the error in the fit are given in Table 2. Note that $\langle t \rangle$ increases linearly with either $1 + r_e/r_r$ (small $\langle N \rangle$) or $1/\nu$ (large $\langle N \rangle$) according to the following expressions

$$\langle t \rangle = 0.008(1 + r_e/r_r)\exp(1.33^{d/\langle L \rangle}), \quad \text{Group A, B, C, D} \tag{14}$$

$$\langle t \rangle = (0.0003/\nu)\exp(1.46^{d/\langle L \rangle}), \quad \text{Group E, F, G, H} \tag{15}$$

The goodness of fit, estimated by the mean absolute fractional deviation $\langle |t_m - t_d|/t_d \rangle$, where t_m is the curve fit en-

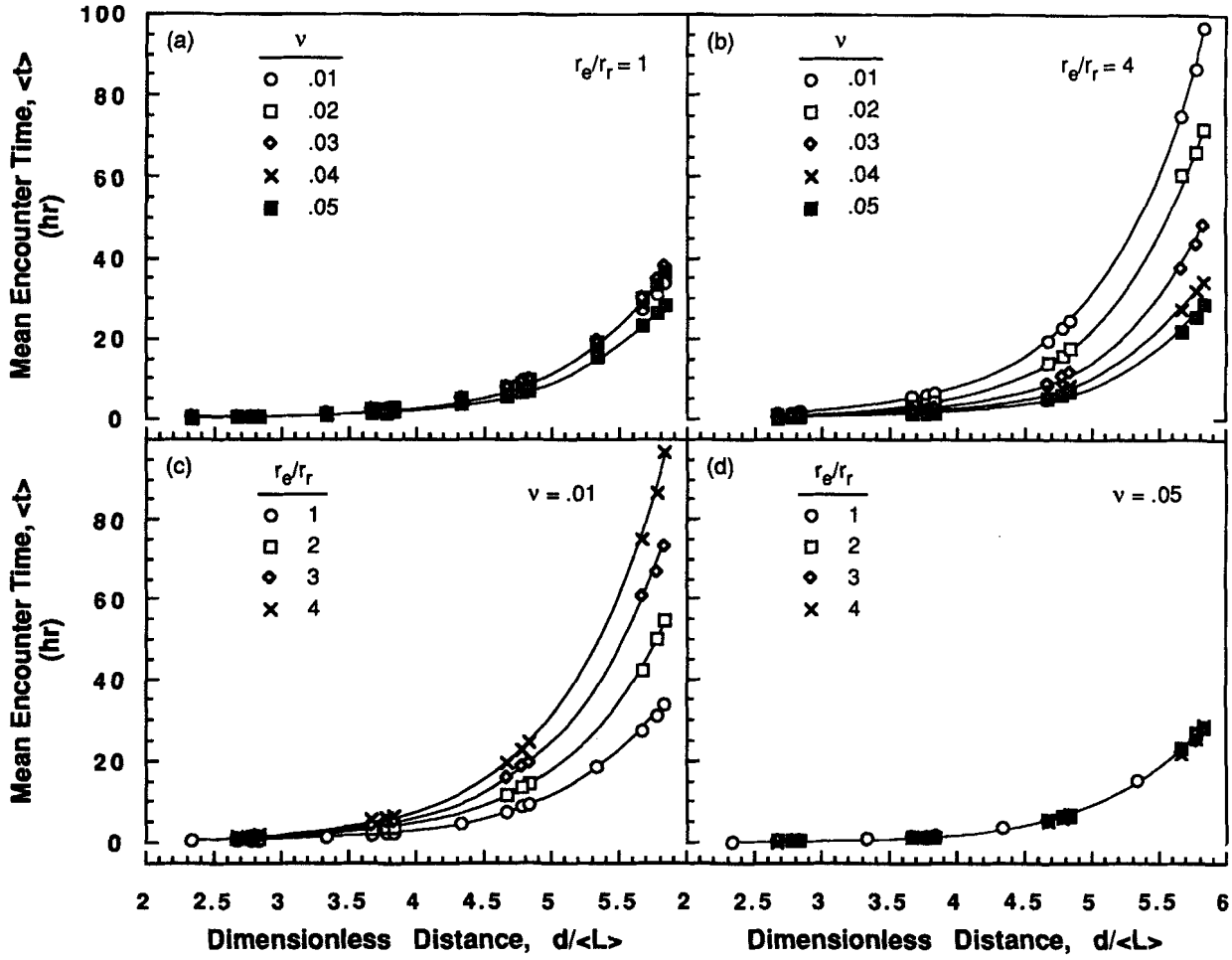

Figure 5. Extremes of behavior in the mean encounter time with changes in the rate of initiation ν and the ratio of extension to retraction rates r_e/r_r.

(a) For the smallest ratio $r_e/r_r = 1$, little variation is seen with changes in ν; (b) as the ratio r_e/r_r increases, the effect of ν increases. The maximum effect was seen at the maximum ratio $r_e/r_r = 4$. Encounter time decreases with increasing ν, the greatest sensitivity occurring at small ν; (c) at small ν, increasing r_e/r_r produces significant increases in the encounter time; (d) as ν increases, the effect of r_e/r_r decreases. At the maximum value examined $\nu = 0.05\ s^{-1}$, results at different values of r_e/r_r fell along the same curve. This was also true at $\nu = 0.04\ s^{-1}$ (not shown).

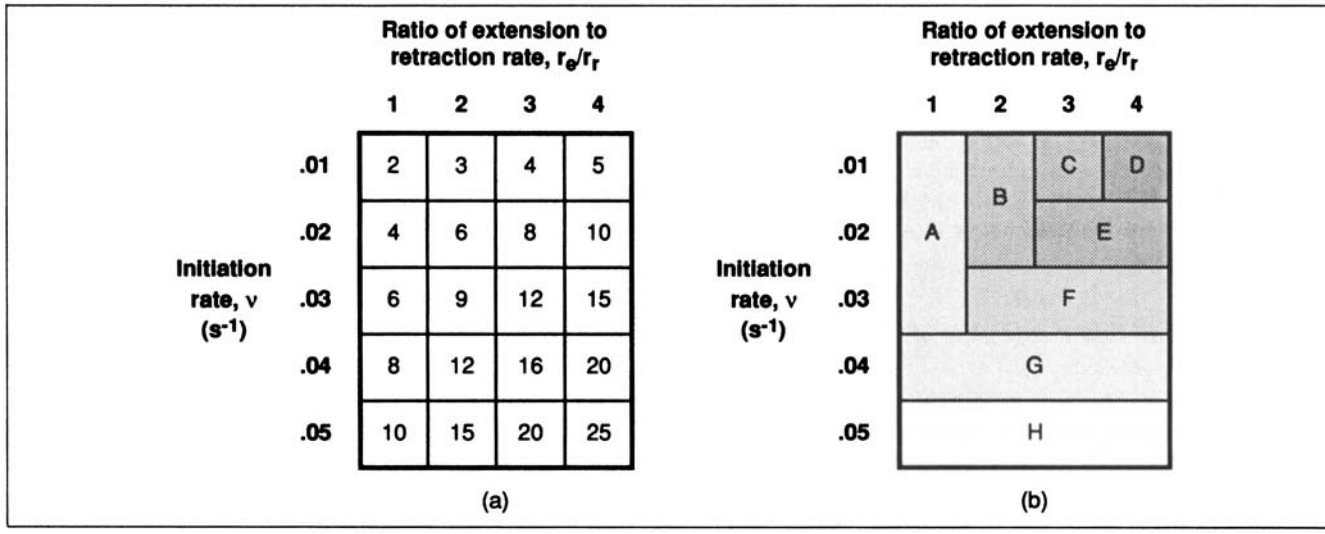

Figure 6. (a) Mean number of filopodia per growth cone corresponding to a given value of ν and r_e/r_r; (b) regions of parametric sensitivity in the parameter space for $d/\langle L \rangle > 2$.

Parameter combinations within a given letter group yielded mean encounter times that were indistinguishable from one another. In general, encounter times decreased from upper right to lower left.

Table 2. Parameters Fitting Simulation Results for $d/\langle L\rangle > 2$ to Eq. 13

Region	a	b	$\langle\lvert t_m - t_d\rvert/t_d\rangle$
A	1.3315	0.015542	0.0227
B		0.023539	0.0202
C		0.031622	0.0156
D		0.039649	0.0097
E	1.4573	0.015276	0.0280
F		0.009928	0.0318
G		0.007417	0.0420
H		0.005838	0.0480

counter time and t_d is the corresponding simulated encounter time, reflected less than 5% deviation in the curve fit to any of the data. The relationships in Eqs. 13–15 are empirical only and are provided for the sake of convenience in predicting encounter times. A variety of other curves were unable to provide a more satisfactory fit for either the entire range of $d/\langle L\rangle$ or $d/\langle L\rangle > 2$.

Mean encounter time curves are shown in Figure 7 ($d/\langle L\rangle > 2$) and Figure 8 ($d/\langle L\rangle < 2$). Results in Figure 7a are shown on a time scale of several days. Smaller portions of the plot in Figure 7a are expanded in Figure 7b to 7c to show time scales of one day (Figure 7b) and several hours (Figure 7c). Times up to several hours are of significance for in vitro assays of filopodial encounter, as well as many in vivo events. Experimental considerations have generally limited the observation of systems involving filopodial encounter, and detailed observation has been possible only in vitro or in invertebrates, in which development is rapid. Thus, an upper limit of meaningful encounter times has not been established. Encounter occurred in less than 30 min for all cases in which $d/\langle L\rangle < 2$ (Figure 8).

Effect of the distribution of maximum extension times

An indication of the effect of encounter due to the distribution of maximum filopodial extension time was obtained by changing the parameter α (Eq. 2) from 2 to 5 while keeping

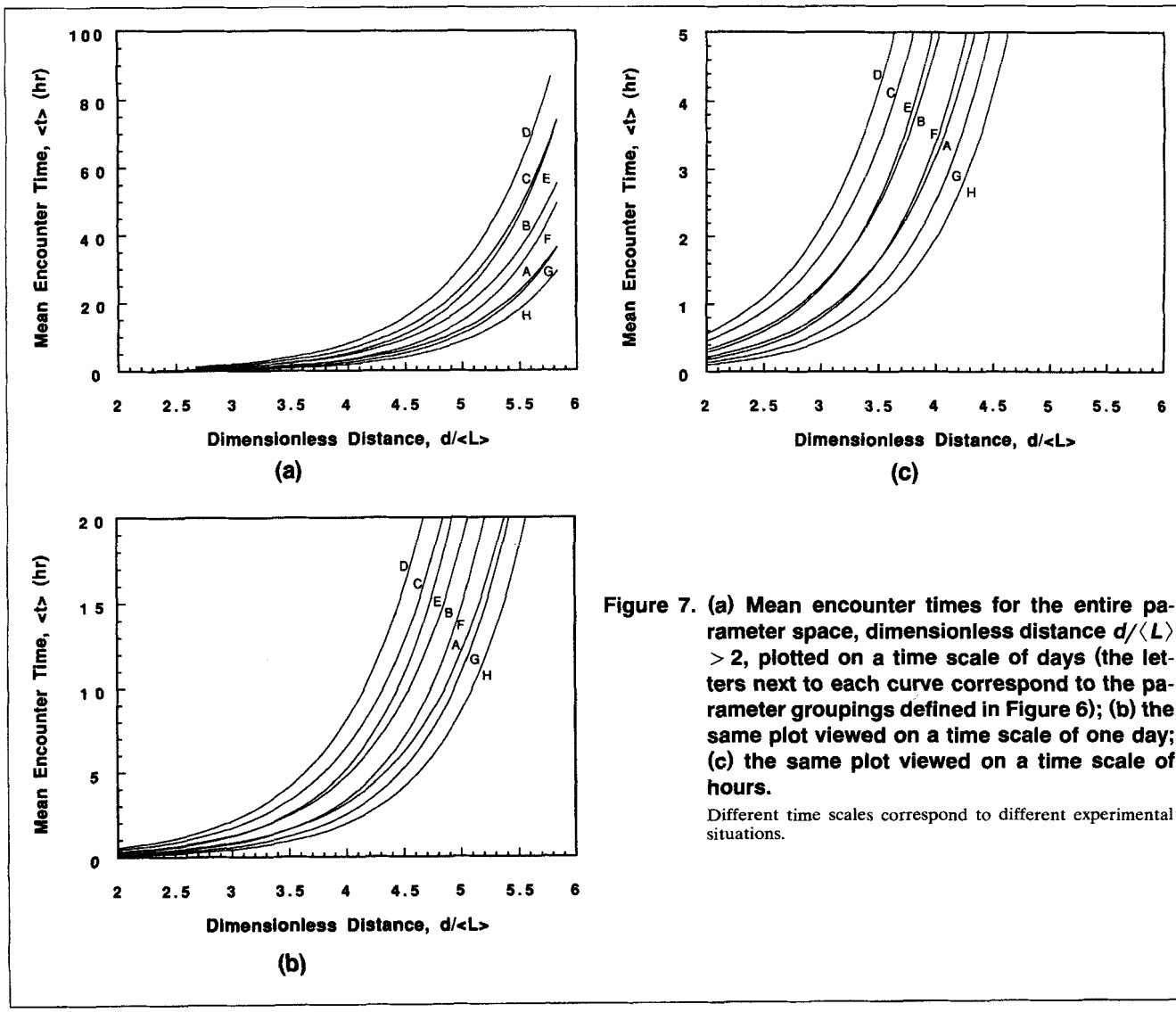

Figure 7. (a) Mean encounter times for the entire parameter space, dimensionless distance $d/\langle L\rangle > 2$, plotted on a time scale of days (the letters next to each curve correspond to the parameter groupings defined in Figure 6); (b) the same plot viewed on a time scale of one day; (c) the same plot viewed on a time scale of hours.

Different time scales correspond to different experimental situations.

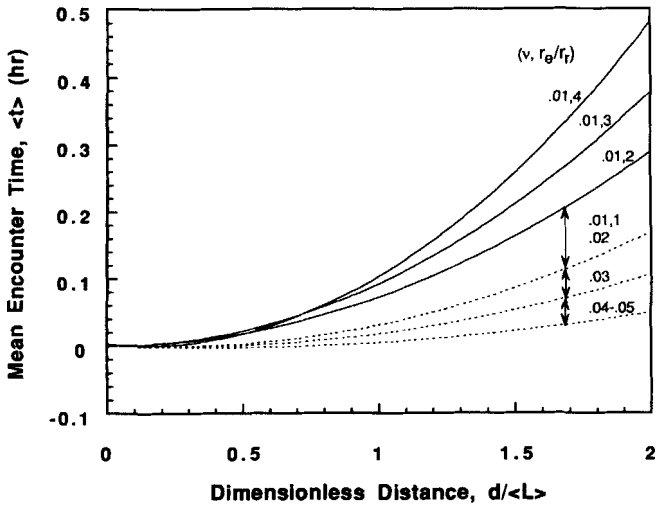

Figure 8. Mean encounter times for the entire parameter space, dimensionless distance $d/\langle L\rangle < 2$.

Top three curves each represent a single condition indicated by the values (ν, r_e/r_r) next to each curve. The dashed curves indicate bounds on regions encompassing the parameter combinations indicated. Only the value of ν is given when a region includes all values of r_e/r_r for that ν.

the mean α/β constant. The resulting range of encounter times was shifted primarily to the left of those obtained for $\alpha = 2$ (Figure 9). The gamma probability distribution, used to characterize maximum filopodial extension time, becomes more symmetrical as the parameter α increases. To maintain the same value of α/β, β must increase, which shifts the density of the distribution to the left. This increases the probability of moderately short filopodia, resulting in generally shorter encounter times at values of $d/\langle L\rangle$ less than about 3, and sharply increased times at longer distances.

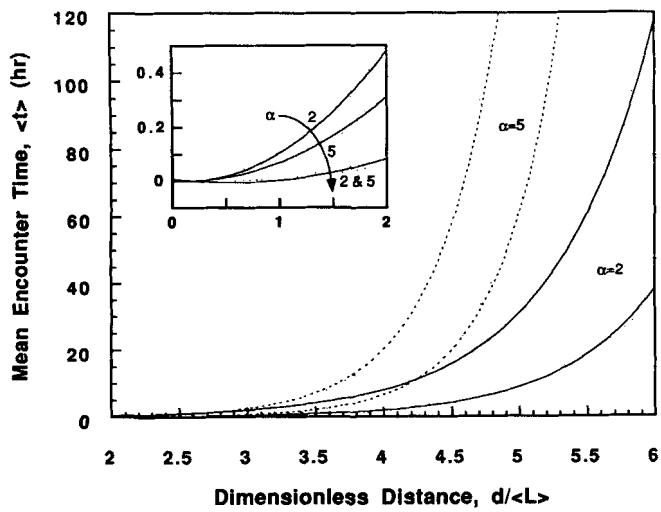

Figure 9. Effect of change in the distribution of filopodial lifetimes on the range in encounter times.

Changing the shape parameter α from 2 to 5 while holding the mean α/β constant shifts the distribution towards shorter filopodia and produces a sharp increase in encounter times above $d/\langle L\rangle = 3$.

Discussion

Multiple mechanisms are believed to guide the growing nerve axon to its destination, but the lack of fundamental descriptions for individual guidance events has made it difficult to develop a quantitative picture of the guidance process. In this article, a simulation model of filopodial dynamics has been employed to characterize a key step in many guidance scenarios, the encounter between filopodium and target. The results obtained from the simulation suggest that the most important factor in filopodial-target encounter in the absence of growth cone migration is the number of filopodia generated per unit time with access to the target. This depends on both geometry and kinetics, and not simply on the average number or length of filopodia per growth cone, measures often presumed to indicate the growth cone's ability to detect the presence of guidance cues.

The system geometry employed for the simulation addresses the situation in which the target can be viewed as an infinite strip separated from the growth cone by a fixed distance d. *In vivo*, such a target may represent a segment boundary in the embryonic tissue (O'Connor et al., 1990; Caudy and Bentley, 1986; Figure 2a), fascicle of other axons (Myers and Bastiani, 1993a), or other extended regions of extracellular cues (Dodd and Jessell, 1988). *In vitro*, targets of this geometry are commonly encountered as a second chemical (Clark et al., 1993; Hammarback and Letourneau, 1986; Lom et al., 1993) or physical (Clark et al., 1987) region in a binary patterned substrate (Figure 2b to 2c). The assumption that the growth cone maintains a constant distance to the target is appropriate either when growth cone approach to the target is slow relative to the characteristic time of filopodial-target encounter, or when growth cone movement occurs only parallel to the target boundary (Clark et al., 1993; Figure 2b), thus preserving the separation distance d. Although the simulation addresses targets with a rectangular geometry that are large relative to the growth cone, the rules elucidated from this study lend insight into several relevant modifications of the target geometry (Figure 10). From the above observation that filopodia in the sectors to either side of the one centered at 0° do not contribute significantly to the encounter time until the number of sectors increases to about 8, it is reasonable to expect that the same encounter times would be observed for rectangular targets of any dimensions centered about the x-axis when $\langle N\rangle < 8$. For larger values of $\langle N\rangle$, as the target size decreases, adjacent filopodia that would have encountered a larger target are unable to make contact with the smaller one, leading to an increase in encounter time. Another target geometry of interest is a circular shape, with a dimension ranging down to that of the growth cone when the target is a single cell, for example (O'Connor et al., 1990; Caudy and Bentley, 1986; Bentley and Caudy, 1983). As in the preceding case, when $\langle N\rangle < 8$, the encounter times presented here should be essentially unchanged for a circular target centered about the x-axis and at the same separation distance from the growth cone, regardless of the target size. Again, at larger values of $\langle N\rangle$, encounter times can be expected to increase with decreasing target diameter. In reality, filopodia are not perfectly constrained to a radial extension from their initiation site, nor do they initiate at discrete positions around the growth cone. Thus, there will be some finite minimum target size for which

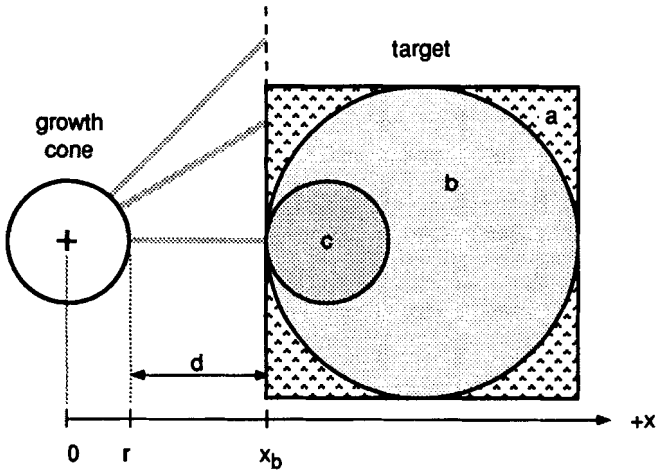

Figure 10. Other relevent target geometries, for which the current results can be interpreted under appropriate conditions.

(a) Rectangular target with arbitrary finite dimension; (b) rounded target with arbitrary finite dimension; (c) rounded target with dimension similar to that of the growth cone. For $\langle N \rangle < 8$, encounter time is determined primarily by the filopodium at 0°, and hence will be similar to the results for a semi-infinite rectangular target in all three cases. As adjacent filopodia contribute more to target encounter, decreasing target size and rounded geometry lead to an increase in the mean encounter time over those presented here.

the results presented here apply, even for $\langle N \rangle < 8$. Such deviations generally occur on a scale somewhat smaller than the growth cone, suggesting a minimum target size on the order of the growth cone diameter.

The simulation results are in accord with existing experimental evidence, though only preliminary or indirect comparison is possible with currently available data. A number of studies have indicated that the strategic placement of spatial cues can serve to attract the migrating growth cone along a desired pathway. For example, the growth of pioneer axons in the limb bud of the grasshopper embryo follows a path marked by several intermediate guidance targets. Filopodial encounter with these targets occurs quickly as the growth cone approaches the target at a distance approximately equal to the average filopodial length (O'Connor et al., 1990; Caudy and Bentley, 1986), though the exact distance varies, as expected for a probabilistic encounter. Filopodial involvement in growth cone guidance has also been argued on the basis of changes seen in filopodial structure and dynamics with changes in extracellular environment. Growth cones elaborate their filopodia at key decision points in the embryo (Holt, 1989; Tosney and Landmesser, 1985; Raper et al., 1983; Taghert et al., 1982), and exhibit significant filopodial changes in response to guidance targets (Berman et al., 1993; Myers and Bastiani, 1993b), specific growth substrates (Payne et al., 1992), neurotransmitter (Haydon et al., 1984), chemical factors regulating Ca^{++} influx (Rehder and Kater, 1992; Mattson and Kater, 1987), and electrical fields (Davenport and McCaig, 1993; Davenport and Kater, 1992). The results presented here support the notion that such alternations may serve to vary the sensitivity of the growth cone to the presence of guidance cues by altering the probability of filopodial-target encounter. Figure 5 shows regions of both parametric sensitivity and parametric insensitivity in the encounter time for the relatively narrow parameter space known to apply to growth cone migration. This provides for a wide range in encounter times with only subtle changes in filopodial dynamics in some regions of the parameter space, i.e., at high r_e/r_r or low ν, while smoothing out the variability in regions of low r_e/r_r or high ν. Although little is known yet about the values of these parameters in guidance vs. nonguidance situations, it is easy to imagine, as an example, growth cones in a noninstructive environment having low rates of filopodial initiation that are boosted by factors in the neighborhood of key pathfinding decisions, enhancing the probability of filopodial encounter with guidance cues. As filopodial initiation picks up and encounter becomes more certain, however, an increased sensitivity to guidance cues would seem unnecessary past a certain point, while a decrease could be advantageous for limiting the variability in encounter times. The level of flexibility afforded by this or other possible scenarios supported by the simulation results for directing growth cone migration is consistent with the complexity known to be required to achieve the highly specific patterning of the nervous system. At the same time, the simulation results contradict the implicit assumption that has been made in most experimental studies of growth cone filopodial dynamics, which have focused primarily on measuring the average filopodial number and length, and correlating these to growth cone behavior. As Figures 6 to 7 indicate, these mean quantities do not necessarily correspond directly to target encounter, nor do they reveal how the dynamic quality of filopodial behavior may contribute to the growth cone response.

Comparison of simulation results with current experiments highlight several needs that must be addressed before the model can be validated and fully utilized. First, it is essential that filopodial dynamics be measured in sufficient detail to test Eqs. 8 and 11 and to evaluate the simulation of filopodial structure on the basis of statistical measures. Characterization of filopodial dynamics remains sketchy at present, as reflected in Table 1. Extension and retraction rates have been determined on several occasions (Buettner et al., 1994; Myers and Bastiani, 1993b; O'Connor et al., 1990; Sheetz et al., 1990, 1992; Argiro et al., 1985; Bray and Chapman, 1985) and generally support the assumption of linear growth and shortening, though nonlinearity (Argiro et al., 1985), pauses, and multiple alternating extension and retraction phases have also been observed (Myers and Bastiani, 1993b). Far fewer measurements of filopodial initiation rate (Buettner et al., 1994; Bray and Chapman, 1985) or maximum extension time (Buettner et al., 1994) have been reported. Filopodial orientation, shown here to be a key factor in determining encounter time, can vary considerably with extracellular conditions and there is evidence that other parameters of filopodial dynamics vary with filopodial position on the growth cone (Myers and Bastiani, 1993b). Both of these features will require further characterization. A second experimental need is the observation and measurement of filopodial encounter events. The current study provides guidelines for designing experiments for this purpose. As Figure 7a shows, encounter times ranging from minutes to days can be achieved within the parameter space that applies here. Under experimental conditions, both in vivo and in vitro systems often deteriorate

in a matter of hours, making the observation of longer encounter times unfeasible. In addition, the shorter the encounter time the larger the number of events that can be observed. On the other hand, parametric sensitivity is greatly diminished if the encounter time becomes too small, with contact occurring in less than 5 min for most conditions when $d/\langle L\rangle < 2$. Based on these considerations, target distances of 3–3.5 times $\langle L\rangle$ appear to be an ideal choice in many cases. Finally, to further address the role of filopodial-target encounter in growth cone guidance, it will be necessary to determine the link between encounter and detection. In its current form, the model describes target contact by a single filopodium. However, it is possible that detection occurs at a higher contact threshold or involves receptor-mediated phenomena that do not correspond simply to a contact criterion. Insight into questions such as these will require the observation of sequences of filopodial encounter-growth cone response and the hypothesis of mechanisms that connect these events.

In summary, this work has produced a quantitative model that serves as a starting point for investigating filopodial mediation of growth cone guidance. The mathematical relationships for the mean filopodial number and length and the simulation results for the mean encounter time represent hypotheses of the model that can be tested directly against experiment. In addition, they provide a means to suggest nonintuitive consequences of altering filopodia dynamics and to pinpoint the subcellular effects of experimental treatments that modify filopodial structure. The mathematical framework can be further expanded to provide a link between molecular events, cellular structure and function. In this way, it serves as a basis for a comprehensive, mechanistic model of filopodial-mediated growth cone guidance that may lend insight into the filopodial behavior of many other cell types as well.

Acknowledgments

This work was supported by a grant from The Whitaker Foundation.

Notation

d = distance from growth cone to target, μm
f_i = fraction of filopodia with lifetime T_{L_i}
L = filopodium length as a function of time, μm, Eq. 4
$L_{\max}$ = maximum extension length of an individual filopodium, μm
m_e = notation for $m_{i,e}$ when $m_{i,e}$ is constant for all i
m_i = number of time intervals for which filopodium with lifetime T_{L_i} exists
$m_{i,e}$ = number of time intervals for which filopodium of maximum length $L_{\max_i}$ extends
$m_{i,r}$ = number of time intervals for which filopodium of maximum length $L_{\max_i}$ retracts
$p(\cdot)$ = probability density function for time to reach maximum extension, Eq. 2, number of filopodia per growth cone, Eq. 9, or filopodial lifetime
r_e = rate of filopodial extension, μm/s
r_r = rate of filopodial retraction, μm/s
t = time since initiation of an individual filopodium
t_d = simulated mean encounter time at a given value of $d/\langle L\rangle$
t_i = time to initial filopodium contact by the ith growth cone in a simulated population
t_m = curve fit mean encounter time at a given value of $d/\langle L\rangle$
$\langle t\rangle$ = mean encounter time, h
T_L = lifetime of an individual filopodium
$T_{\max}$ = time for an individual filopodium to reach maximum extension, s
$\langle T_{\max}\rangle$ = mean time to maximum filopodial extension, s
$\langle T_r\rangle$ = mean filopodial retraction time
x_b = x-coordinate of target boundary

Greek letters

θ = angle of filopodial projection relative to leading front of growth cone
$\Gamma(\cdot)$ = gamma function
ν = rate of filopodial initiation, s^{-1}
σ_N^2 = variance in the number of filopodia per growth cone, Eq. 8

Literature Cited

Argiro, V., M. B. Bunge, and M. I. Johnson, "A Quantitative Study of Growth Cone Filopodial Extension," *J. Neurosci. Res.*, **13**, 149 (1985).

Bentley, D., and M. Caudy, "Pioneer Axons Lose Directed Growth After Selective Killing of Guidepost Cells," *Nature*, **304**, 62 (1983).

Bentley, D., and A. Toroian-Raymond, "Disoriented Pathfinding by Pioneer Neurone Growth Cones Deprived of Filopodia by Cytochalasin Treatment," *Nature*, **323**, 712 (1986).

Berman, S. A., D. Moss, and S. Bursztajn, "Axonal Branching and Growth Cone Structure Depend on Target Cells," *Dev. Biol.*, **159**, 153 (1993).

Bray, D., and K. Chapman, "Analysis of Microspike Movements on the Neuronal Growth Cone," *J. Neurosci.*, **5**, 3204 (1985).

Buettner, H. M., R. N. Pittman, and J. K. Ivins, "A Model of Neurite Extension across Regions of Nonpermissive Substrate: Simulations Based on Experimental Measurement of Growth Cone Motility and Filopodial Dynamics," *Dev. Biol.*, **163**, 407 (1994).

Caudy, M., and D. Bentley, "Pioneer Growth Cone Steering Along a Series of Neuronal and Nonneuronal Cues of Different Affinities," *J. Neurosci.*, **6**, 1781 (1986).

Chien, C.-B., D. E. Rosenthal, W. A. Harris, and C. E. Holt, "Navigational Errors made by Growth Cones without Filopodia in the Embryonic Xenopus Brain," *Neuron*, **11**, 237 (1993).

Clark, P., S. Britland, and P. Connolly, "Growth Cone Guidance and Neuron Morphology on Micropatterned Laminin Surfaces," *J. Cell. Sci.*, **105**, 203 (1993).

Clark, P., P. Connolly, A. S. G. Curtis, J. A. T. Dow, and C. D. W. Wilkinson, "Topographical Control of Cell Behaviour," *Development*, **99**, 439 (1987).

Cohan, C. S., "Frequency-Dependent and Cell-Specific Effects of Electrical Activity on Growth Cone Movements of Cultured Helisoma Neurons," *J. Neurobiol.*, **21**, 400 (1990).

Davenport, R. W., and S. B. Kater, "Local Increases in Intracellular Calcium Elicit Local Filopodial Responses in Helisoma Neuronal Growth Cones," *Neuron*, **9**, 405 (1992).

Davenport, R. W., and C. D. McCaig, "Hippocampal Growth Cone Responses to Focally Applied Electric Fields," *J. Neurobiol.*, **24**, 89 (1993).

Dodd, J., and T. M. Jessell, "Axon Guidance and the Patterning of Neuronal Projections in Vertebrates," *Science*, **242**, 692 (1988).

Hammarback, J. A., and P. C. Letourneau, "Neurite Extension Across Regions of Low Cell-Substratum Adhesivity: Implications for the Guidepost Hypothesis of Axonal Pathfinding," *Dev. Biol.*, **117**, 655 (1986).

Hardin, J., and D. R. McClay, "Target Recognition by the Archenteron during Sea Urchin Gastrulation," *Dev. Biol.*, **142**, 86 (1990).

Haydon, "Serotonin Selectivity Inhibits Growth Cone Motility and Synaptogenesis of Specific Identified Neurons," *Science*, **226**, 561 (1984).

Holt, C. E., "A Single-Cell Analysis of Early Retinal Ganglion Cell Differentiation in Xenopus: from Soma to Axon Tip," *J. Neurosci.*, **9**, 3123 (1989).

Letourneau, P. C., "Cell-Substratum Adhesion of Neurite Growth Cones and its Role in Neurite Elongation," *Exp. Cell Res.*, **124**, 127 (1979).

Letourneau, P. C., T. A. Shattuck, and A. H. Ressler, "Branching of Sensory and Sympathetic Neurites in Vitro is Inhibited by Treatment with Taxol," *J. Neurosci.*, **6**, 1912 (1986).

Letourneau, P. C., T. A. Shattuck, and A. H. Ressler, "'Pull' and 'Push' in Neurite Elongation: Observations on the Effects of Different Concentrations of Cytochalasin B and Taxol," *Cell. Motil. Cytoskel.*, **8**, 193 (1987).
Lom, B., K. J. Healy, and P. E. Hockberger, "A Versatile Technique for Patterning Biomolecules onto Glass Coverslips," *J. Neurosci. Meth.*, **50**, 385 (1993).
Marsh, L., and P. C. Letourneau, "Growth of Neurites without Filopodial or Lamellipodial Activity in the Presence of Cytochalasin B," *J. Cell Biol.*, **99**, 2041 (1984).
Mattson, M. P., and S. B. Kater, "Calcium Regulation of Neurite Elongation and Growth Cone Motility," *J. Neurosci.*, **7**, 4034 (1987).
Morse, P. M., *Queues, Inventories and Maintenance*, Wiley, New York (1958).
Myers, P. Z., and M. J. Bastiani, "Cell-Cell Interactions During the Migration of an Identified Commissural Growth Cone in the Embryonic Grasshopper," *J. Neurosci.*, **13**, 115 (1993a).
Myers, P. Z., and M. J. Bastiani, "Growth Cone Dynamics during the Migration of an Identified Commissural Growth Cone," *J. Neurosci.*, **13**, 127 (1993b).
O'Connor, T. P., J. S. Duerr, and D. Bentley, "Pioneer Growth Cone Steering Decisions Mediated by Single Filopodial Contacts *in situ*," *J. Neurosci.*, **10**, 3935 (1990).
Oakley, R. A., and K. W. Tosney, "Contact-Mediated Mechanisms of Motor Axon Segmentation," *J. Neurosci.*, **13**, 3773 (1993).
Olkin, I., L. J. Gleser, and C. Derman, *Probability Models and Applications*, Macmillan, New York (1980).
Payne, H. R., S. M. Burden, and V. Lemmon, "Modulation of Growth Cone Morphology by Substrate-Bound Adhesion Molecules," *Cell Motil. Cytoskel.*, **21**, 65 (1992).
Raper, J. A., M. Bastiani, and C. S. Goodman, "Pathfinding by Neuronal Growth Cones in Grasshopper Embryos. I. Divergent Choices Made by the Growth Cones of Sibling Neurons," *J. Neurosci.*, **3**, 20 (1983).
Rehder, V., and S. B. Kater, "Regulation of Neuronal Growth Cone Filopodia by Intracellular Calcium," *J. Neurosci.*, **12**, 3175 (1992).
Sheetz, M. P., N. L. Baumrind, D. B. Wayne, and A. L. Pearlman, "Concentration of Membrane Antigens by Forward Transport and Trapping in Neuronal Growth Cones," *Cell*, **61**, 231 (1990).
Sheetz, M. P., D. B. Wayne, and A. L. Pearlman, "Extension of Filopodia by Motor-Dependent Actin Assembly," *Cell Motil. Cytoskel.*, **22**, 160 (1992).
Taghert, P. H., M. J. Bastiani, R. K. Ho, and C. S. Goodman, "Guidance of Pioneer Growth Cones: Filopodial Contacts and Coupling Revealed with an Antibody to Lucifer Yellow," *Dev. Biol.*, **94**, 391 (1982).
Tosney, K. W., and L. T. Landmesser, "Growth Cone Morphology and Trajectory in the Lumbosacral Region of the Chick Embryo," *J. Neurosci.*, **5**, 2345 (1985).

Appendix

Mean filopodial length

The mean filopodial length per growth cone is determined by averaging the instantaneous mean length over M time intervals

$$\langle L\rangle = [\ \mathfrak{L}_1/N_1 + \ \mathfrak{L}_2/N_2 + \cdots + \ \mathfrak{L}_M/N_M\ ] \div M \quad \text{(A1)}$$

where $\mathfrak{L}_j$ is the sum of the N_j individual filopodial lengths present during the jth time interval and M is large. If we consider the ith filopodium, initiated during the $(s-1)$st time interval and present through the $(s+m_i-1)$st interval, the sum of its contributions to the mean filopodial length over its lifetime is given by

$$L_i = [l_{is}/N_s + l_{i,s+1}/N_{s+1} + \cdots + l_{i,s+m_i-1}/N_{s+m_i-1}] \div M \quad \text{(A2)}$$

where l_{ij} is the length of the ith filopodium during the jth time interval. Its mean contribution over its lifetime is L_i/m_i, which tends to a mean value

$$(\Sigma L_i/m_i)/Q \to \langle L\rangle_i \quad \text{(A3)}$$

when calculated for a large number of filopodia Q with the same lifetime m_i.

Since extension and retraction are linear and occur between the same limits, i.e., l_{ij} takes on values between 0 and $L_{\max_i}$ in both cases, this relationship holds for each phase as well, with the number of time intervals in the filopodium lifetime m_i replaced by the number of extension or retraction time points $(m_{i,e}+1)$ or $(m_{i,r}+1)$, respectively. Thus, we can develop an expression for $\langle L\rangle_i$ by considering one phase alone. The following treatment is presented in terms of the extension phase.

If the ith filopodium extends for $m_{i,e} = m_e$ constant time intervals for length Δt then

$$l_{ij} = r_e \cdot [j-(s-1)]\Delta t \quad j = s-1, s, \ldots, m_e + s - 1 \quad \text{(A4)}$$

and

$$L_i/(m_e+1) = r_e \cdot \Delta t(1/N_s + 2/N_{s+1} + \cdots + m_e/N_{s+m_e-1})_i \div [M\cdot(m_e+1)] \quad \text{(A5)}$$

where the subscript i on the sum in parentheses indicates the fact that the enclosed sequence of values for N_j occurs during the lifetime of the ith filopodium. Summing the contributions of all Q filopodia with the same maximum length $r_e \cdot m_e \Delta t$, during M time intervals produces an expression with $Q \cdot m_e$ terms

$$\Sigma L_i/(m_e+1) = \Sigma r_e \cdot \Delta t(1/N_s + 2/N_{s+1} + \cdots + m_e/N_{s+m_e-1})_i \div [M\cdot(m_e+1)], \quad i = 1,2,\ldots,Q \quad \text{(A6)}$$

with s varying randomly from 1 to $M - m_i$ for the different values of i. However, not all the N_j will be unique. Assuming k distinct values, denoted by lowercase n_j to indicate the fact that j no longer represents the time interval but simply a different value of the filopodial number per growth cone

$$\langle L\rangle_i = r_e \cdot \Delta t[(q_{11}/n_1 + q_{12}/n_2 + \cdots + q_{1k}/n_k) + (2q_{21}/n_1 + 2q_{22}/n_2 + \cdots + 2q_{2k}/n_k) + \cdots + (m_e q_{m_e 1}/n_1 + m_e q_{m_e 2}/n_2 + \cdots + m_e q_{m_e k}/n_k)] \div [M\cdot(m_e+1)] \quad \text{(A7)}$$

where q_{rj} is the total number of filopodia in their rth extension interval when the number of filopodia per growth cone is n_j. Since filopodial extension is independent of the number of filopodia per growth cone, the number of filopodia in their ith extension interval should not differ for different values of n_j when M is large; hence, $q_{1j} = q_{2j} = \cdots = q_{m_e j} = q_{je}$, and we can write

$$\langle L\rangle_i = r_e \cdot \Delta t(1+2+\cdots+m_e)(q_{1e}/n_1 + q_{2e}/n_2 + \cdots + q_{ke}/n_k) \div [M\cdot(m_e+1)] \quad \text{(A8)}$$

Substituting $q_{je} = n_j \cdot p(n_j)M$

$$\langle L\rangle_i = r_e \cdot \Delta t(1+2+\cdots+m_e)/(m_e+1) \times [p(n_1)+p(n_2)+\cdots+p(n_k)] \quad \text{(A9)}$$

or

$$\langle L\rangle_i = (1-p_o)r_e \Delta t\, m_e/2 \quad \text{(A10)}$$

where $p(n_j)$ is the probability that a growth cone has n_j filopodia, and p_o is the probability of a growth cone with zero filopodia. Since $L_{\max_i} = r_e m_e \Delta t$, this yields

$$\langle L\rangle_i = (1-p_o)L_{\max_i}/2 \quad \text{(A11)}$$

The mean filopodial length per growth cone is now obtained from a time-weighted average of the mean lengths for all possible values of $L_{\max}$

$$\langle L\rangle = f_1 \cdot \langle L\rangle_1 + f_2 \cdot \langle L\rangle_2 + \cdots + f_i \cdot \langle L\rangle_i + \cdots \quad \text{(A12)}$$

where each $\langle L\rangle_i$ is weighted by the fraction of filopodial lifetimes contributed by filopodia with a lifetime T_{L_i}

$$f_i = T_{L_i} p(T_{L_i}) / \Sigma T_{L_i} p(T_{L_i}) \quad \text{(A13)}$$

Assuming a continuum of values for T_{L_i}, Eq. A12 becomes

$$\langle L\rangle = (1/2)(1-p_o)\int L_{\max} T_L\, p(T_L)\, dT_L / \int T_L\, p(T_L)\, dT_L \quad \text{(A14)}$$

Since $T_L = (1 + r_e/r_r)T_{\max}$ is a linear transformation, $p(T_L)$ is a gamma distribution with the same form as $p(T_{\max})$, and $(1 + r_e/r_r)$ factors out everywhere in the numerator and denominator (Olkin, 1980); substituting $L_{\max} = r_e T_{\max}$, Eq. A14 can be rewritten

$$\langle L\rangle = (1/2)(1-p_o)r_e \int (T_{\max})^2 p(T_{\max})\, dT_{\max} / \int T_{\max}\, p(T_{\max})\, dT_{\max} \quad \text{(A15)}$$

Equation A15 evaluates to (Olkin, 1980)

$$\langle L\rangle = (1-p_o)r_e \Gamma(\alpha+2)/2\beta\Gamma(\alpha+1) \quad \text{(A16)}$$

or

$$\langle L\rangle = (1-p_o)r_e(\alpha+1)/2\beta. \quad \text{(A17)}$$

Manuscript received Feb. 10, 1995, and revision received June 7, 1995.